Geophysical Monitoring of Foam used to Deliver Remediation Treatments within the Vadose Zone

Yuxin Wu[1], Susan Hubbard[1], Dawn Wellman[2]

[1] Earth Sciences Division, Lawrence Berkeley National Laboratory, 1 Cyclotron Rd, Berkeley, CA 94720

[2] Environmental Systems Group, Pacific Northwest National Laboratory, PO Box 999 Richland, WA 99352

Abstract

Foam is a promising vehicle for delivering amendments into the vadose zone for *in situ* remediation; it is an approach being considered for *in situ* treatment and stabilization of metals and radionuclides located within the deep vadose zone of the Department of Energy (DOE) Hanford site, WA. A central aspect of evaluating the effectiveness of this approach is the ability to monitor foam distribution, its transformation, and the reactions that it induces in the subsurface, ideally in a non-invasive manner. In this study, we performed laboratory experiments to evaluate the potential of geophysical methods (complex resistivity and time domain reflectometry, TDR) as tools for monitoring foam assisted amendment delivery in the deep vadose zone. Our results indicated great sensitivity of electrical methods to foam transportation and evolution in unsaturated porous media that were related to foam bubble coalescence and drainage processes. Specifically, we observed (1) a decrease of electrical resistivity (increase of electrical conductivity) by over an order of magnitude in both silica sand and natural sediment matrices during foam transportation; (2) an increase of resistivity (decrease of conductivity) by over two fold during foam coalescence and drainage; (3) a distinct phase and imaginary conductivity signature related to the evolution of water films on sediment grains during foam injection and evolution processes. To assist with the interpretation of these data, TDR measurements were used to monitor moisture content, which provided complementary information about foam distribution and drainage. Our results clearly demonstrated the sensitivity of electrical and TDR signals to foam transportation and

evolution in unsaturated porous media and suggested the potential of these methods for monitoring the response of a system to foam based remediation treatments at field scales.

Abbreviations: EDL, electrical double layer; IP, induced polarization; EM, electromagnetic; TDR, time domain reflectometry

Introduction

The vadose zone is a critical conduit for transport of pollutants from the ground surface to ground water. Contaminants in the vadose zone are susceptible to mobilization through diffusion or during recharge and water table fluctuations, posing a long-term threat to groundwater. Effective remediation of vadose zone contaminants is one of the greatest challenges in environmental remediation (Looney and Falta 2000; Zhong et al. 2010, and references therein). This challenge is exacerbated in deep vadose zone environments, where surface excavation and offsite treatment is economically unfeasible. In the deep vadose zone, conventional amendment delivery strategies, which rely on injection of water based solutions, are fraught with hydrologic and geochemical challenges. Preferential flow in the deep vadose zone is pervasive (Hendrickx and Flury 2001), which often leads to preferential percolation of injected treatment through permeable pathways that often bypass the most contaminated regions (Glass et al. 1988; Zhong et al. 2009). Furthermore, the application of large volumes of fluid can potentially mobilize contaminants in the vadose zone, enhancing their transport to the underlying aquifers (Hanson et al. 1993; Qafoku et al. 2003; Qafoku et al. 2007).

There are several attractive characteristics of using foam to deliver remedial treatments to the vadose zone. Foam is defined as a two phase system in which gas bubbles are separated by thin liquid films (Birkerman 1973). It has higher viscosity compared to water or gas phase alone and has been used in the oil industry to enhance sweep efficiency during oil recovery (Smith 1988; Hirasaki 1989). Using foam as a delivery vehicle can enhance the infiltration efficiency of remedies by promoting sweeping efficiency in low permeable zones (Yan et al. 2006). Also, the flow of foam can potentially be better controlled through manipulation of pressure gradients in the subsurface (Zhong et al. 2009). Moreover, the use of foam as a delivery vehicle significantly reduces the volume of water required, thus mitigating contaminant mobilization to the groundwater through water flushing.

Successful development of foam as a remedial treatment delivery vehicle requires understanding of the foam dynamic behavior in heterogeneous porous media. For example, can foam be delivered to a target contaminated location prior to the collapse of

the foam bubbles? Can the foam bubble size be optimized for transportation in sediments having a known pore size distribution? When the bubbles collapse, might drainage be significant enough that it could mobilize contaminants downward? These and other questions are currently being addressed by researchers such as Zhong et al. (2010).

An additional consideration is associated with the ability to monitor and eventually predict the delivery, emplacement, and long term performance of foam *in situ*, as needed to evaluate the treatment performance. Conventional techniques for subsurface remediation monitoring rely on wellbore based approaches to collect samples or make measurements. Because of their limited spatial extent, these methods often only provide limited information for the understanding of key controls on subsurface flow and transport. This is especially true in the vadose zone, where vertical infiltration pathways can form as a result of variable saturation and heterogeneity and where fluid recovery during sampling can be challenging.

The application of geophysical methods to improve the characterization and monitoring of near subsurface properties and remediation processes has gained much interest in recent years (Rubin and Hubbard 2005). Because geophysical data can be collected from many platforms (such as at the ground surface, between wellbores, and within wellbores), these methods can interrogate the subsurface variables over a variety of spatial scales and resolutions. One of the main advantages of using geophysical monitoring over conventional measurements is its ability to provide spatially extensive information about the subsurface in a minimally invasive manner at a comparatively high resolution. A particularly attractive feature of geophysical methods for subsurface process monitoring is its ability to collect a suite of continuous datasets at the same location as a function of time, or 'time-lapse' datasets that can illuminate changes in the system. Time-lapse geophysical approaches have been effectively used for hydrological investigations to monitor vadose zone water infiltration at the The Department of Energy (DOE) Hanford site and elsewhere (Hubbard et al. 1997a; Hubbard et al. 1997b; Binley et al. 2002; Daniels et al. 2005; Kowalsky et al. 2005; Lambot et al. 2006; Rucker et al. 2011). Time-lapse geophysical methods have also been successfully used to monitor biogeochemical transformations associated with remediation treatments (Williams et al. 2005; Hubbard et

al. 2008; Williams et al. 2009; Wu et al. 2010; Wu et al. 2011). Together, these studies have demonstrated the potential of geophysical methods – particularly time-lapse complex conductivity (or resistivity) and TDR methods - for improving our understanding of amendment distribution, induced biogeochemical reactions, and the underlying control of heterogeneity on subsurface environmental remediation processes.

In this study, we performed laboratory experiments to evaluate the applicability of geophysical methods as tools for monitoring foam transportation and evolution in vadose zone sediments. This is a prelude to field-scale geophysical monitoring of a foam-based remedial pilot study that is planned for a deep vadose zone contaminated site at Hanford (Zhong et al. 2010). We explore the sensitivity of both electrical and TDR signals to foam transportation and subsequent transformations and investigate if the methods are suitable tools for monitoring foam delivery assisted subsurface remediation at the field scales.

Theoretical background

For this study, we focused on exploring complex conductivity (or resistivity) and TDR methods based on their predicted sensitivities to major changes during foam injection and transformation, mostly moisture content and interfacial properties of mineral/water/air. Complex conductivity (σ^*) measures charge conduction behavior and for a porous geological medium it is often times frequency dependent. The measured $\sigma^*(\omega)$ can be represented as,

$$\sigma^*(\omega) = \sigma'(\omega) + i\sigma''(\omega) \qquad (1)$$

where ω is the angular frequency, σ' is the measured real part of $\sigma^*(\omega)$, being the conduction component; σ'' is the measured imaginary part of $\sigma^*(\omega)$, being the induced polarization (IP) component and $i = \sqrt{-1}$.

The factors that contribute to the complex conductivity signatures vary depending on sample conditions. For saturated media, electrical charge transport is primarily determined by (1) the electrolytic conduction (σ_{el}) via interconnected fluid-filled pore space (a purely real term), and (2) a complex interfacial conduction (σ^*_{int}), occurring near

the grain/electrolyte interfaces. The σ_{el} is dependent on the conductivity of the electrolyte (σ_w) saturating the porous media (Archie 1942) whereas σ^*_{int} represents an interfacial charge conduction and polarization behavior within the electrical double layer (EDL) at the grain/electrolyte interface (Schwarz 1962; Wong 1979; Slater et al. 2005). For partially saturated vadose zone material with negligible metal content (which is the case we studied here) the dominant electric pathway is through water films on mineral surfaces. As such, the real (or charge conduction) component of the electrical signal is mainly determined by the number and thickness of these water film paths, their continuity and tortuosity and the salinity of the fluid in the films.

Although only a few studies have explored the imaginary (or charge polarization) component of the electrical signal in unsaturated media, a positive correlation between induced polarization and water content has been documented (Parkhomenko 1971; Titov et al. 2004; Ulrich and Slater 2004). Foam systems inherently provide a significant amount of gas bubbles and, therefore, air/water interfaces. Potential polarization at these interfaces should be considered because of the existence of negative surface charges at air/water interfaces based on zeta potential measurements (Manciu and Ruckenstein 2006; Creux et al. 2007). Previous research has investigated the potential effect of the air/water interface on electrical resistivity (Knight 1991) and has suggested that conduction at air/water interface might be responsible for resistivity hysteresis effects observed during drainage and imbibition. However, to the best of our knowledge, no study has investigated low frequency charge polarization behavior at this interface.

Based on these previous findings, our conceptual model of the complex conductivity (or resistivity) response to foam injection in a porous media is as follows. When foam is injected into a porous media, in addition to the growth of the water films on sediment grains due to moisture content increase, the newly introduced water films that exist between the foam bubbles will serve as additional conduits for charge conduction, thereby causing an increase in electrical conductivity (or decrease in resistivity). As the foam coalesces and the bubbles grow in size in time, the number and thickness of these conduits within pore space will decrease, thus leading to a decrease of conductivity (increase of resistivity). Foam injection and subsequent coalescence and drainage could alter charge polarization in two ways: (1) by changing the thickness and extensiveness of

the water films on sediment grains or (2) by changing the volume of air/water interfaces that are charged, which could contribute to overall charge polarization.

TDR, a commonly used electromagnetic (EM) method, measures the apparent dielectric permittivity of a medium based on the measured velocity of a guided EM wave. With this approach, an EM signal is sent to a waveguide and travels along the rods in transverse electromagnetic mode. With known length of the probe and travel time, EM wave velocity can be calculated, which can be used to estimate dielectric properties. A commonly used petrophysical model for estimating water content from dielectric constant values is the complex refractive index model (Birchak et al. 1974):

$$\sqrt{\kappa} = \theta\sqrt{\kappa_w} + (\phi - \theta)\sqrt{\kappa_a} + (1 - \phi)\sqrt{\kappa_s}, \quad (2)$$

where θ is water content. ϕ is porosity and κ_w, κ_a, κ_s and κ are dielectric constants of water, air, sediments and the bulk sample. Another well used relationship between dielectric permittivity and water content is the empirical Topp's equations. The general Topp's equation (Topp et al. 1980) is given as

$$\kappa = 3.03 + 9.3\theta + 146\theta^2 - 76.7\theta^3. \quad (3)$$

As foam is introduced into low moisture content porous media, we expect the moisture content to increase, thereby increasing the dielectric constant and decreasing the propagation velocity. Subsequent bubble transformations could cause additional changes in the moisture content if drainage occurs during bubble coalescence and growth.

Materials and Methods

Experimental Apparatus

Two apparatus were built for the experiments: one for TDR and the other for complex resistivity measurements (Figure 1).

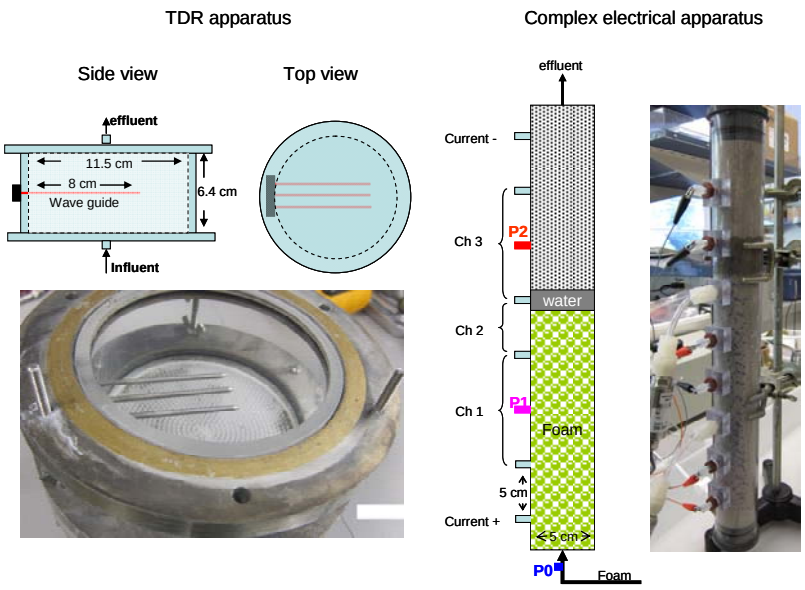

Figure 1: Apparatus design for TDR (left) and complex resistivity (right) measurements. P0, P1 and P2 are the locations of the pressure transducers used for pressure monitoring. The cartoon of the electrical column indicates a single time point, where foam is traveling from the bottom to the top of a sand-packed column and where a water front has formed at the advancing front of the foam plume.

The TDR apparatus is made from polycarbonate and is a short and wide column with a dimension of 6.4 cm (height) by 11.5 cm (inner diameter, I.D.) An 8 cm buriable waveguide with three stainless steel rods was installed in the middle of the column for guiding radar wave propagation during TDR measurements. Polycarbonate filter plates (with ~ 1 mm pore size) were installed at both ends of the column to help confine the sediments as well as distribute the injected foam evenly across the column before entering the sediments. The column for complex resistivity measurements had a dimension of 44 cm (height) by 5 cm (I.D.). Eight ports with an interval of 5 cm were installed along the side wall of the column for electrical measurements and pressure monitoring. Electrical signals were measured at three different channels (1, 2 and 3 from bottom to top; Figure 1), and pressure was monitored at three different locations using pressure transducers (P0, P1 and P2; Figure 1).

Solid matrix

To investigate the effects of different moisture retention capacities on foam behavior and geophysical signals, both silica sand and Hanford site sediments were used for the experiments. Ottawa sand was first used in both columns followed by Hanford site sediments. Ottawa sand with fairly uniform grain size at ~ 600 μm was acquired from US Silica (Ottawa, IL) and the average porosity of Ottawa sand packed column is ~38%. Site sediments used in the experiments were acquired from boreholes close to the DOE Hanford site BC cribs area. The sediments used in this research are the same K2 sediment used in Zhong et al (2010), which are primarily sand with silt and clay. These sediments have an average porosity of 29.6%, with a mean grains size and standard deviation of 1180 μm and 150 μm, respectively. The Hanford sediments have larger average grain size, lower porosity, and poorer sorting relative to the Ottawa sand. Because the Ottawa sand surface is relatively smooth and has fewer fines and micro pores compared to the Hanford sediments, low moisture retention capacity was expected for the silica sand samples.

Surfactant and foam generation

The foaming agent is a water based solution of a surfactant mix including cocamidopropyl betaine, coconut diethanolamide and sodium lauryl sulfate (Stepan Company, IL). This solution was blended in a modified Blender (L'equip 306500 RPM) with continuous supply of nitrogen as the gas component of the foam. The size of the produced foam bubble is dependent on the blending rate; a 800 RPM blending rate was used to produce a ~200 μm average bubble size for this study. The size of the foam bubble was confirmed with optical microscope. The fresh foam produced from this setup was primarily ball shaped with a volumetric water content of ~10-15% or equivalently, a foam quality of 90-85%. The produced foam was then introduced into the measurement apparatus driven by gas pressure or by using a peristaltic pump.

Optical imaging of foam evolution

Imaging using an optical microscope (Motic DM143, Xiamen, China) was carried out to help understand foam evolution after being injected. A silicon tubing (2 mm I.D) was

placed under the microscope horizontally and freshly generated foam was injected into the tube and was observed and photographed over time to document foam transformation after injection.

Experimental Procedure

For both TDR and electrical measurements, three scenarios were tested: foam only; foam in silica sand packed columns and foam in site sediments packed columns. For the foam only scenario, pure foam was injected into the empty columns and electrical and TDR measurements were collected regularly over time. The columns were subsequently cleaned, dried and packed with Ottawa sand. During packing, the columns were tapped a few times after each ~ 1 cm of sand was introduced. The sand was very dry with negligible moisture content (< 0.5 %). After packing, foam was introduced into the bases of both columns and injection continued until steady foam flow was observed for at least 10 minutes at the effluent ends. TDR and complex resistivity measurements were collected continuously before, during, and after foam injection into the Ottawa sand columns. In the final experiment, the columns were cleaned and repacked with Hanford sediments using the same procedure described above. The sediments had initial moisture content at ~ 3-4% based on gravimetrical measurements. Foam was injected into the columns at ~ 12 ml/min using peristaltic pump. For all three scenarios, foam was injected into the apparatus from the bottom and was continued until stable foam was eluded from the top of the apparatus for at least 10 minutes.

Complex resistivity and TDR measurement approaches

Electrical measurements were collected with a National Instruments dynamic signal analyzer (DSA, NI 4461) at the three different channels (Channel 1,2 and 3) using Ag/AgCl electrodes placed along the length of the electrical column (Figure 1). A preamplifier was used to boost the input impedance to 10^9 Ohm to avoid significant current leakage into the measurement circuitry. Water column based repeatability tests for this system indicate that errors were less than 0.3 mrads for the phase and 0.5% for conductivity when low frequency was used (< 500 Hz). Each measurement was

composed of a phase shift (ϕ) and a magnitude ($|\sigma|$) component. The measurements were recorded relative to a precision reference resistor over thirty frequencies spaced at equal logarithmic intervals from 1 to 1000 Hz. Spectral data below 1 Hz was not recorded because of the short duration of foam transport process within the column (~30 minutes) and the long time required to acquire low frequency (<1 Hz) data. Because the DSA board has only one channel available for sample measurements, a parallel port relay board was built as a multiplexer to switch between the three measurement channels along the length of the column as shown in Figure 1. The data acquisition rate was about 1 dataset per minute; therefore each data cycle for all three channels required ~3 minutes to collect. The real and imaginary components of the complex conductivity represent the magnitude of the conduction and polarization of the sample respectively, and were determined from the following equations:

$$\sigma' = |\sigma| \times \cos\phi \qquad (4)$$

$$\sigma'' = |\sigma| \times \sin\phi \qquad (5)$$

and

$$\phi = \arctan\left(\frac{\sigma''}{\sigma'}\right) \approx \frac{\sigma''}{\sigma'} \quad \text{(When } \phi \text{ is small)} \qquad (6)$$

TDR data were collected with a Trase system (Soilmoisture Equipment Corp, Santa Barbara, CA) using an 8 cm, three prong buriable TDR waveguide probe. The TDR was connected to a multiplexer and programmed to record waveforms every minute. Inflections in the recorded waveform were automatically picked and converted to dielectric constant values. These values were then used with the petrophysical relationship given in Topp's equation (Eq. 3) to estimate moisture content. Ideally, relationships between moisture content and dielectric constant would be developed for each material under consideration (here, the Ottawa sand and Hanford samples). However, with our objective of assessing relative changes in moisture associated with foam injection, coalescence and drainage, the use of an established petrophysical relationship such as Topp's equation was deemed acceptable.

Results and Discussion

We first discuss the results from the optical microscopy study. We then discuss the three experimental column results: the first associated with pure foam only, followed by foam within Ottawa sand, and then foam within the Hanford sediments.

Imaging of Foam Evolution

Foam can only be stable for a certain period of time; coalescence and breakage will eventually occur. Time-lapse optical microscopic observations of foam injected into a horizontal capillary tube illustrate this evolutionary process over a 15 minute timeframe. Figure 2 shows that the freshly injected foam bubbles were dominantly spherically shaped and had an average diameter of ~ 200 μm. With time, the bubbles coalesced and fluid drainage occurred, causing the bubble size growth and the bubble shape change from sphere to polyhedron. Based on tests conducted in tubes of other diameters (5 mm, 25.4 mm and 51 mm; images not shown), the maximum size of the foam bubble is constrained by the size of the pore the bubbles reside.

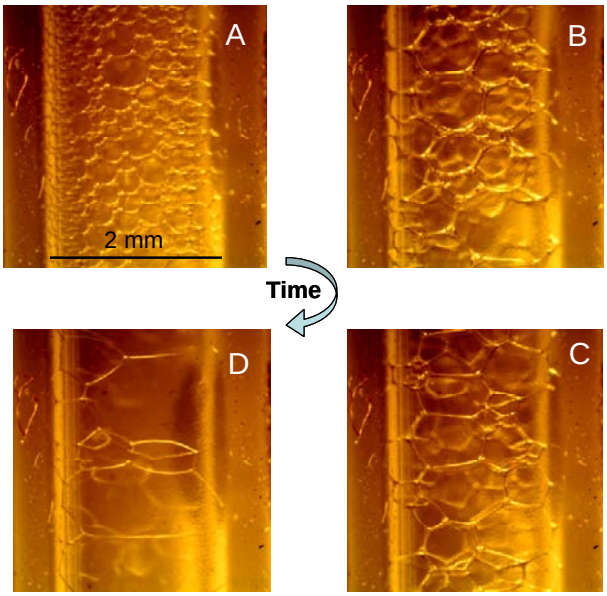

Figure 2: Foam transformation over time after injection within a horizontal 2mm capillary tube stopped. Panel A is the freshly produced foam, Panel B, C, D are snapshots after approximately 5, 10 and 15 minutes.

Based on a conceptual model extracted from the optical microscopy study of foam in a capillary tube, Figure 3 schematically shows the evolution of foam in a low moisture content pore space between grains. The conceptual model assumes that under very low moisture content, water exists as thin films on sediment grains with the pore space filled with air (Figure 3A). Once foam is injected, the pore spaces become filled with ball shaped air bubbles separated by water films and the water saturation of the sediment is greatly enhanced (Figure 3B). Note that bubble breakage and regeneration can occur at pore throats. Therefore, the foam bubbles within the pore space are a mixture of the originally injected and those newly generated during transportation through pore throats. Once foam injection ceased, ball foam bubbles coalesce and transform over time into larger polygons and the excess water drains onto the adjacent sediment grains (Figure 3C). Over time, these polygons become larger (Figure 3D) and will eventually break with all the water absorbed by sediments or drain out.

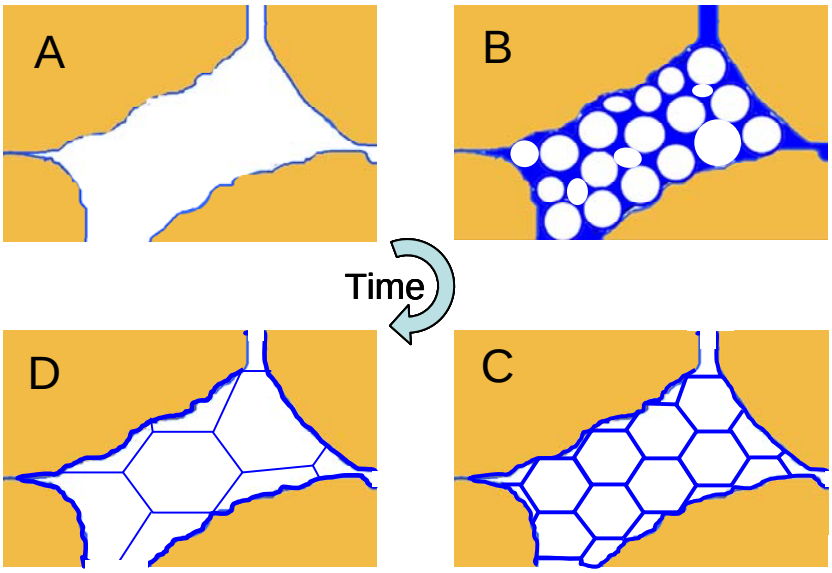

Figure 3: Schematic of foam evolution in pore space: A: baseline pore space filled with air with thin liquid film on sediment grains; B. pore space filled with ball shaped foam during injection phase; C and D: foam transformation from sphere to larger and more polygonal-shaped bubbles.

PURE FOAM PHASE

Foam was produced using the protocol described above and injected into the empty TDR and electrical columns until the columns were filled with the foam. After the columns were completely filled, the injection continued for another ~ 10 minutes to reach stable state. Visually, the transformation in bubble shape and size was apparent over time once foam injection stopped. The original foam had an approximate average diameter of ~ 200 μm and it grew to a few centimeters, constrained by the size of the columns, within about 20 minutes. The evolution of the foam in the two experimental columns was similar based on visual observations although the bubbles grew to larger sizes in the TDR column relative to the electrical column due to the larger diameter of the TDR column. Large changes in both electrical and TDR signals were observed during this process (Figure 4). Electrical resistivity magnitude increased by over two orders of magnitude from ~ 100 ohm.m to over 10,000 ohm.m (Figure 4A). This change is interpreted to be due to the transformation of the fresh, ball-shaped foam bubbles into larger polygons and the concomitant drainage of excess water from the bubble films. This transformation also significantly reduced the number of water films between gas bubbles (i.e. available electric conduits) in the measurement channels, leading to a large resistivity increase. Phase response at 1 Hz from the column is also shown in Figure 4A. No observable phase response was recorded for the initial stage of the experiment, which indicates that the relatively large bubble size (~ 200 μm and larger) provided only limited surface area, which was not significant enough to produce a detectable IP signal. The phase values observed during the later stage of the experiment were likely due to EM coupling because of the large contact resistance between electrodes and the foam during this stage (Figure 4A).

Both the electrical resistivity and moisture responses are consistent with our conceptual model. Moisture content calculated based on TDR measurements revealed a reasonable initial value at ~10%. However, this value dropped to just above zero fairly quickly (Figure 4B), indicating limited resolution of the TDR measurements at low moisture content which is partially due to the short length (8 cm) of the TDR probes. Compared to

TDR measurement, the electrical resistivity provided continuous measurements of resistivity changes during foam transformation even at very low moisture content. Estimation of moisture content based on electrical resistivity can be made upon the establishment of petrophysical correlations between electrical resistivity and moisture content in the context of specific foam characteristics. .

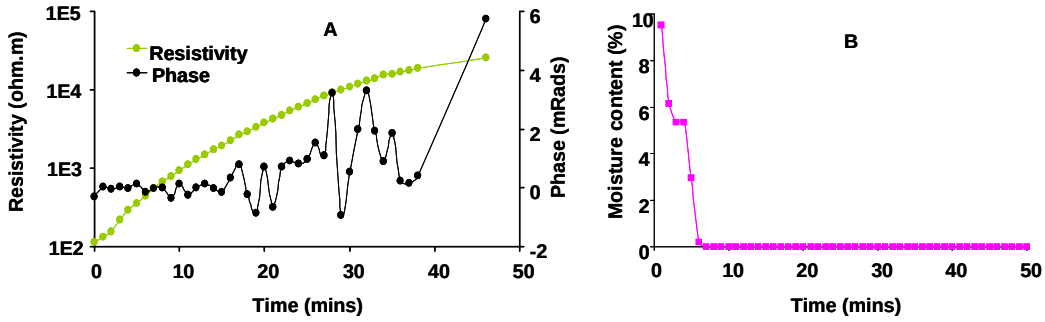

Figure 4: (A) changes of electrical resistivity and phase at 1 Hz (data from channel 1 of the electrical column) and (B) TDR-obtained moisture content after foam injection into the columns.

Foam in silica sand columns

The experimental results from the sand columns are shown in Figure 5 (electrical data) and Figure 6 (TDR data).

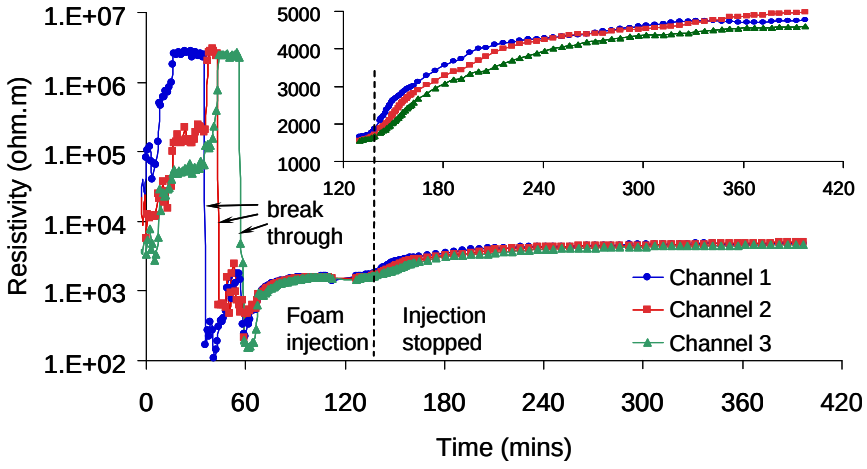

Figure 5: Changes of electrical resistivity magnitude at 1 Hz on log scale during foam injection and transportation in silica sand packed column. Injection started at T = 0 minute. Imbedded figure shows changes of resistivity on linear scale after foam injection stopped at ~130 minutes.

Due to the dryness of the silica sand used in the experiments, the contact resistance between measurement electrodes and the sand was quite high. This caused large noise levels in measurements, therefore large variations in the measured resistivity values of the column before foam arrival at the electrodes (Figure 5). Nevertheless, large resistivity values at >10 K Ωm were observed before the arrivals of the foam at the measurement channels (Figure 5). Foam arrivals at the measurement channels significantly reduced electrical resistivity to ~ 1000 Ωm or below and sequential decreases of the resistivity was observed from channel 1 to 3 (bottom to top) as the foam front migrated sequentially through the measurement channels. Note that between 30 and 60 minutes, there was a short period of resistivity rebound. This rebound was most evident for channel 1, less significant for channel 2 and barely noticeable for channel 3. Although the exact reason warrants further investigation, it might be related to the unsteady breakthrough of the water front at the bottom channels because the water front was thin and uneven in the low part of the column. After the initial foam break through, the resistivity of all three channels started to increase slowly until foam injection stopped at ~ 130 minutes. The imbedded subfigure in Figure 5 shows the changes of resistivity after foam injection ceased, and a resistivity increase from ~ 1500 Ωm to ~5000 Ωm was observed. Note that there was a slight but sequential decrease of the resistivity from channel 1 to 3 (Figure 5) at any given time stamp during foam injection and during most of the post injection stage. This could be related to the characteristics of the water front during its arrival at the three different channels. The water front forms ahead of the foam due to bubble breakage and liquid accumulation and has higher water content than foam itself (Zhong et al. 2009). As the foam travel further into the column and sequentially pass channel 1 to 3, the water front becomes wider and contains more liquid. This resulted in a higher level of saturation of the sand in the upper part of the column (channel 3) relative to the lower part (channel 1), therefore a sequential decrease of electrical resistivity from channel 1 to

3 because resistivity is primarily controlled by saturation level. In addition, effects from initial packing heterogeneity could contribute to the differences in resistivity as well. It is also interesting to note that the resistivity of all three channels increased steadily during continuous foam injection after the foam break through the column. This is also related to the water front because the water front has higher water content than the foam itself, therefore the initial water content of the sand acquired from the arrival of the water front was the highest, i.e. lowest resistivity, right after the breakthrough of the water front (Figure 5). Subsequent arrival and passing of the lower-water-content foam carries some of the liquid away, thus reducing the water content of the sand and is responsible for the increase of resistivity before foam injection stopped. Based on the findings from experiments with pure foam (Figure 4), the gradual increase of electrical resistivity after foam injection has stopped is related to the increase in foam bubble size from foam coalescence and water drainage, i.e. reduction of moisture content as well as the number of available electrical pathways through the water films between gas bubbles.

In addition to large changes in resistivity, we also observed small IP effects due to foam injection into the silica sand matrix; this IP response was recorded after the foam front passed the current injection electrodes at the top (at ~ 65 minutes after injection; Figure 6). A maximum phase response of ~ 4 mrads and imaginary conductivity at 4E-6 S/m were observed during inital foam breakthrough (at ~ 65 minute) and this value gradually dropped to ~ 1 mrads for phase and close to zero for imaginary conductivity during foam coalescence and drainage (T > 130 minutes). Reliable baseline phase and imaginary conductivity data can not be measured before foam arrival at the current electrodes due to large contact resistance between the electrodes and the dry sand. The observed polarization signal during foam injection is due to the formation of water film on sand grains, thus establishing mineral/fluid interfaces and EDL structures, a prerequisite for charge polarization (Lyklema 1995). The EDL is established through surface protonation/deprotonation as well as ion exchange processes on mineral surface when it is in contact with water. The subsequent decrease in phase can be related to the reduced availability of interconnected water films during foam coalescence and drainage.

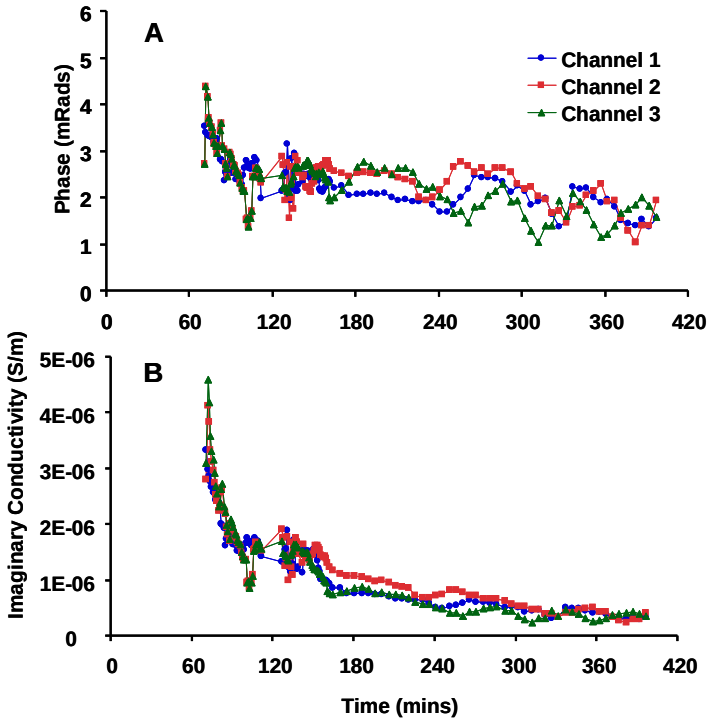

Figure 6: Changes of (A) phase and (B) imaginary conductivity at 1 Hz during foam injection into sand packed columns.

Figure 7 shows changes of moisture content in the TDR column packed with silica sand during foam injection and subsequent transformation. The initial moisture content is close to zero due to the dryness of the sand. During foam injection, a maximal moisture content of ~ 5% was observed, which dropped to a sustained level at ~ 0.5% after the foam injection ceased (Figure 7). The 5% moisture content peak is likely associated with the water front similar to the observation from the electrical column. Interestingly, only a short peak at 5% moisture content was observed which indicates the short thickness of the water front. This is reasonable because the TDR column is short in height and there is only ~ 3 cm between the inlet and the TDR probes, therefore only a thin water front was developed before its arrival at the probes. Also, compared with the electrical column (where the electrical signals were measured across a "distance" between the two potential electrodes which provided a longer resident time of the water front in the measurement area) the TDR probe measures at a single location along the column. As such, the thin

water front is interpreted to have passed by the probes fairly quickly, leading to a short peak of high moisture content.

Experimental data from silica sand packed columns demonstrated the sensitivities of both the complex resistivity and the TDR measurements to foam injection and subsequent transformations. The foam appears to have transported through the column steadily, as evidenced from sequential and significant decreases of resistivity from channel 1 to 3. The water front had higher moisture content compared to foam itself and caused the initial large decrease of the resistivity when it arrived at the measurement channels. This water front was also captured by the TDR measurements as a sharp rise in water content. After the breakthrough of the water front at the electrical and TDR sensors, a resistivity increase and moisture decrease was observed during the subsequent arrival and breakthrough of the foam itself (Figure 5 and 7). The moisture level of the TDR column dropped to a low level at (~ 0.5%) after foam injection has stopped (Figure 7). This is attributed to the low moisture retention capacity of the silica sand, thus the drainage of the excess water accumulated during foam coalescence. The low TDR-obtained final moisture estimates compared relative well with gravimetrically measured value (~0.6% assuming a density of 1 g/ml for surfactant mix) suggesting that the application of the Topp's relation (Equation 4) is reasonable for our study.

These observations are consistent with our conceptual model: foam injected into a porous media causes the growth of water films on sand grains, and the newly introduced water films between gas bubbles serve as additional conduits for charge conduction. Both changes significantly decreased the electrical resistivity (Figure 5), increased the moisture content (Figure 7), and led to a phase response by saturating sand grains with thin water films (Figure 6). During subsequent foam coalescence and bubble size growth, the number and thickness of these water films and charge conduits within pore space decreased, resulted in increase of resistivity and decrease o phase and TDR-estimated moisture content (Figures 5, 6 and 7).

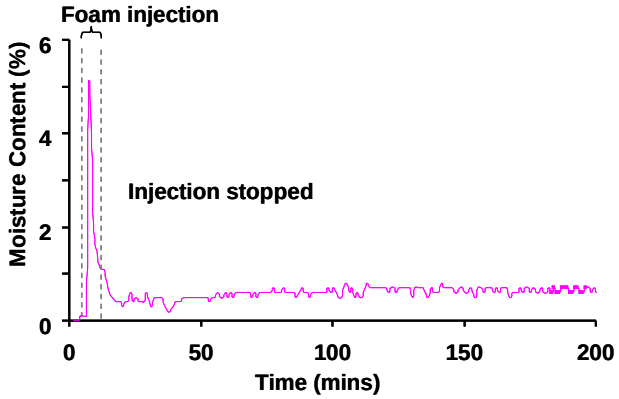

Figure 7: Moisture content changes associated with foam injection into the silica sand packed TDR column.

Foam in Hanford Site Sediments

In the last experiment with Hanford sediments, pressure data at three different locations (inlet, 1/3rd and 2/3rd of the column, Figure 1) were collected for the electrical column and are shown in Figure 8. The inlet pressure increased continuously to ~ 40 pound per square inch (PSI) as foam transported further into the column during injection. Pressure at one third and two thirds of the distance from the bottom of the column increased to ~32 PSI and 16 PSI, respectively. Figure 8 also shows the pressure responses associated with the different phases of the experiment. Pressure started to increase upon the arrival of the foam at the individual pressure sensors and increased consistently for all three locations until the foam break through the top of the column at ~ 34 minutes after injection started (Figure 8). A slight increase of pressure was observed at all three locations during continuous injection after foam break through the top of the column. This slight increase of pressure is potentially related to the increase of moisture content of the sediment due to water adsorption during this period which may enhance pressure requirement for foam transportation. Because the effluent port was kept open, the pressures started to decrease slowly after injection stopped over time at all three locations, indicating bubble coalescence and slow gas release from the effluent end of the column.

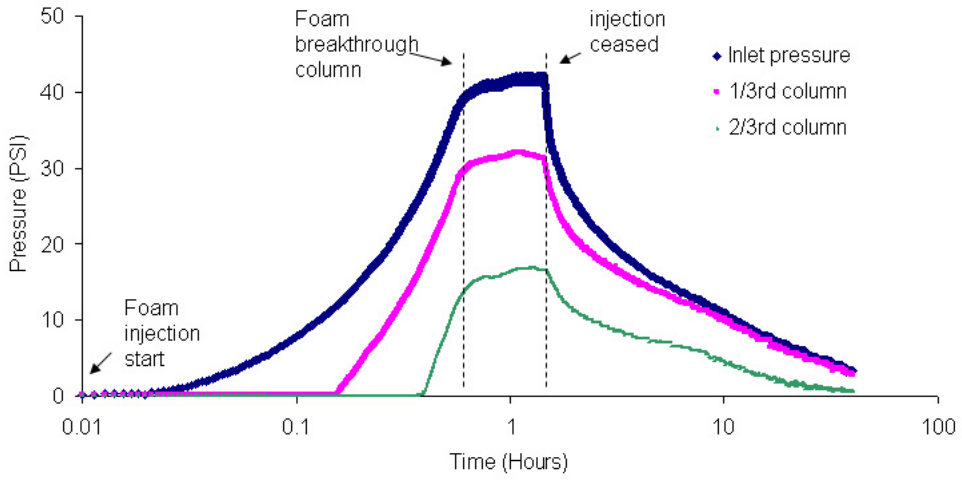

Figure 8: Pressure at three different locations during foam injection into the Hanford-sediment packed column.

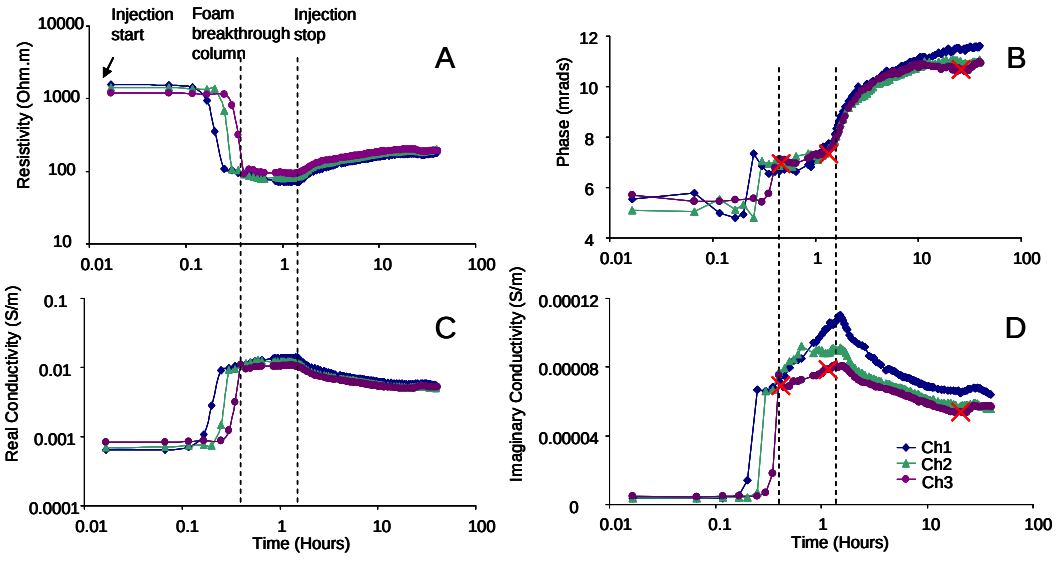

Figure 9: Electrical measurements at 1 Hz during foam injection into sediment packed column: A: resistivity magnitude; B: phase; C: real conductivity and D: imaginary conductivity. Note that resistivity and real conductivity are plotted on log scale. The red crosses marked the time stamps (0.45, 1.1 and 17.6 hours) where spectral responses will be presented and discussed below.

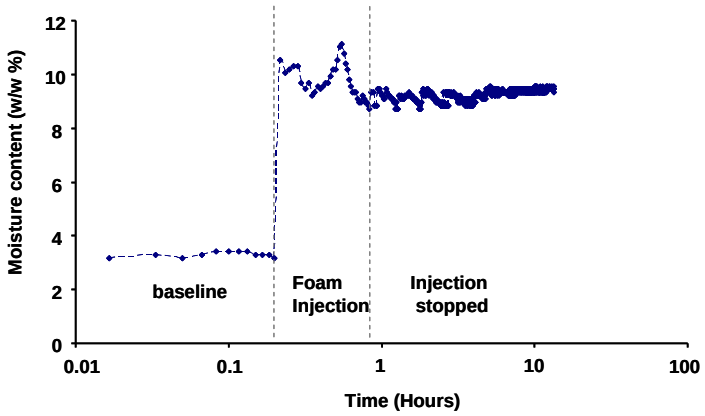

Figure 10: Moisture content change during foam injection into sediment packed column calculated from TDR measurements.

Electrical data at 1 Hz collected during this experiment are shown in Figure 9 and moisture content calculated from the TDR column run in parallel with the electrical column is shown in Figure 10. Our discussion will focus on the electrical column, for which the experiment can be divided into three different phases (Figure 9): (1) An injection phase from 0 - ~ 0.5 hours where foam was injected upward from the bottom of the column and eventually breakthrough at the top of the column; (2) A stable foam injection phase from 0.5 - 1.5 hour, and (3) A post injection/coalescence phase after 1.5 hours.

Distinctive electrical signals were observed during the three different phases of foam injection. During the initial injection phase, the resistivity decreased from > 1000 Ωm to <100 Ωm sequentially across channels 1-3 (Figure 9A) and real electrical conductivity increased by an order of magnitude from 0.001 S/m to ~ 0.01 S/m (Figure 9C). In addition to changes in resistivity and conductivity, there is a slight phase increase from ~ 5.5 mrads to 7 mrads during foam injection and a large increase in imaginary conductivity by over an order of magnitude from ~4E-6 S/m to ~7E-5 S/m. After breakthrough of the foam at the top of the column, continuous but much slower decrease of resistivity (increase of real conductivity) was observed during extended foam injection. Slight increases of phase and imaginary conductivity were also observed during this

period. It is interesting to note that the resistivity behavior during the continuous foam injection phase is different in the site sediment packed column relative to the sand packed column: The resistivity continued to decrease in the site sediment column while it started to increase in the sand column. This could be related to the different moisture retention capabilities between site sediment and Ottawa sand. Due to high moisture retention capacity, the site sediment continued to absorb liquid and increased its moisture content during foam injection until a stable moisture level is achieved, leading to a continuous resistivity decrease before foam injection was stopped. However, during continuous foam injection after the arrival of the water front, Ottawa sand started to lose some of its moisture, previously acquired from the water front, due to its low moisture retention capacity, leading to a resistivity increase during this process. After the foam injection ceased, slow but continuous rebound of resistivity and real conductivity were observed in the site sediment column similar to the observation from the sand column. Phase continued to increase but imaginary conductivity started to decrease during this post injection period.

TDR measurements indicated that the baseline moisture content of the sediment was ~3.2% before foam injection which quickly increased to ~ 10% during foam injection and then reached a sustained value of ~ 9% for the rest of the experiment. Gravimetrical water content analysis of samples recovered from the electrical column showed a moisture content at ~ 10%, similar to the TDR-based estimates.

The different measurements lead to an integrated interpretation of the foam behavior in porous material. During the injection phase, the large decrease of resistivity over one order of magnitude is attributed to the growth of water films on sediment grains as well as the addition of new water films (i.e. electrical conduits) between gas bubbles within the pore space as illustrated in Figure 3B. The large increase of imaginary conductivity is indicative of increased extensiveness and interconnectivity of water films on sediment grains due to moisture content increase during foam injection, thus increasing wetted surface area and their connectivity available for charge conduction and polarization. A small electrical phase increase was observed during this period as well. Electrical phase magnitude is roughly the ratio between imaginary and real conductivity (Equation 6), both of which increased simultaneously during foam injection. Because the rate of

increase for imaginary conductivity was slightly higher than that of the real conductivity, a small increase of the phase response was observed.

During stable foam injection after its breakthrough at the top of the column, the resistivity continued to decrease slowly and the real conductivity, phase and imaginary conductivity continued to increase. During this stage, the bulk pore spaces were filled with foam bubbles and can be considered relatively stable. The major change during this stage was the continuous hydration of the sediments and the increase of the magnitude of the water films and probably their thickness and interconnectivity. Imaginary conductivity (Figure 9D) is exclusively related to the conduction and polarization along these water films and its continuous increase can be considered evidence of water film growth during this stage. As mentioned above, the continuous hydration of the soil particles is interpreted to be responsible for the slight decrease of resistivity (increase of conductivity) during this period. We also attribute the slight increase of phase to be due to hydration effects. After foam injection ceased, all electrical parameters reverted toward initial conditions except phase response, which continued to increase. Changes of electrical signatures during this stage were related to the coalescence of the foam bubbles. As discussed previously on the silica sand column and shown in Figure 3C and 3D, the number and thickness of water films (i.e. electrical conduits) between gas bubbles decreased during foam coalescence and resulted in an increase of resistivity and decrease of the conductivity. Note that the resistivity never recovered back to the baseline value because the water released from bubble coalescence was absorbed by adjacent soil particles, maintaining its moisture content at a higher level, thus enhanced electrical conductivity relative to the baseline. The coalescence and breakage of the foam bubbles could disrupt the connectivity between sediment grains previously enhanced by the water films between foam bubbles. This could reduce the interconnectivity of the water films on sediment grains, therefore reducing the amount of interconnected surface available for charge polarization, thus, the magnitude of surface conduction and polarization, i.e. imaginary conductivity, along these water films. During this stage the real conductivity decreased faster than the imaginary conductivity, causing an increase of the phase response, the ratio between the two. The sustained moisture within the column during this stage is confirmed by the TDR measurements (Figure 10). Note that the TDR response

for the sediment packed column is dramatically different from that of the sand packed column (Figure 5). While moisture content of the sand column decreased significantly due to low moisture retention capacity during bubble coalescence and drainage, moisture level was sustained in the sediment packed column. This is an indication that site sediment has a much higher moisture retention capacity relative to the Ottawa sand and that water released from foam coalescence and breakage was absorbed by adjacent sediment grains, thus maintaining higher moisture content in the longer term.

Discussion of the complex resistivity data has focused on those collected at 1 Hz because this is the frequency at the typical range used for field scale IP surveys thus interpretation of the experimental results at this frequency is indicative of the expected responses from field scale applications. However, spectral responses from 1 to 1000Hz were collected during the experiments and examples of spectral phase and imaginary conductivity data from channel 3 at selected times (0.45, 1.1 and 17.6 hours, Figure 9) are shown in Figure 11.

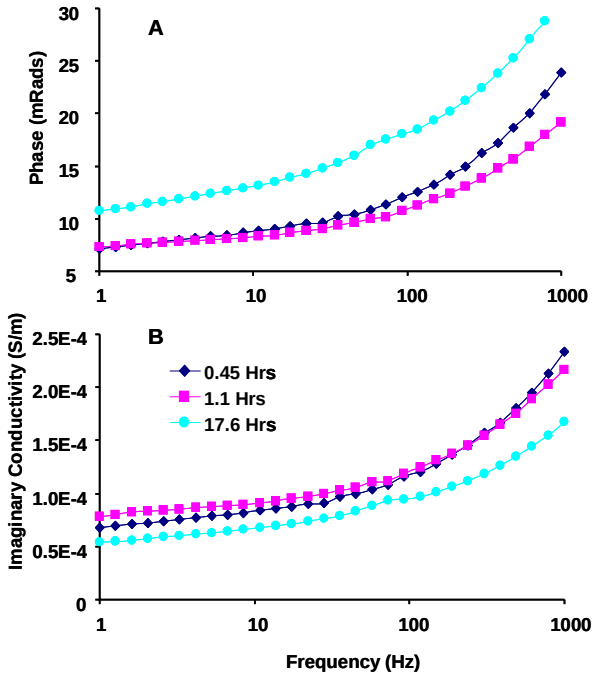

Figure 11: (A) phase and (B) imaginary conductivity spectral data for channel 3 at selected times at 0.45, 1.1 and 17.6 hours from the initiation of foam injection into site sediment packed column.

Spectral responses shown in Figure 11 are representative of all three channels during the experiments. Both phase and imaginary conductivity spectra showed a certain level of frequency dependency with increased values at higher frequencies. However, measurement noise at high frequencies, typically > 100 Hz, from electromagnetic coupling could be high; therefore interpretation of the high frequency data should be exercised with caution. Nevertheless, both phase and imaginary conductivity seem to be weakly frequency dependent and no characteristic critical frequency, i.e. predominant relaxation time length, exists. This type of spectral response has been observed previously for saturated and unsaturated unconsolidated samples (Vanhala 1995; Slater and Lesmes 2002; Ulrich and Slater 2004) and was attributed to superposition of multiple relaxations over various time length scales (Lesmes and Morgan 2001). Note that at low frequency range from 1 to 100 Hz, relative changes between different times are consistent across different frequencies. Therefore, previous analysis of electrical data at 1 Hz is representative of the spectra responses.

Summary and conclusions

A series of column experiments were conducted to measure complex resistivity and TDR signatures during foam injection and evolution to evaluate the potential of these methods for monitoring foam assisted amendment delivery for vadose zone remediation at field scales. Foam was produced by blending surfactant mix under nitrogen atmosphere and was injected into two columns for electrical and TDR monitoring. Three different scenarios were tested: pure foam injection, foam injected into silica sand column and foam injected in site sediment packed column. Complex resistivity and TDR measurements were carried out for all these cases and were compared and related to the foam transportation and evolution processes.

From our experimental results, the following conclusions about the utility of the electrical and TDR methods for monitoring foam distribution and evolution can be made:

- The initial injection of foam into unsaturated porous media (both silica sand and Hanford sediments) resulted in a large decrease of resistivity (increase of

electrical conductivity) due to moisture content increase of the soil particles as well as the addition of newly created water films between gas bubbles within the pore spaces, which act as additional electrical conduits. Continuous foam injection after initial breakthrough results in additional changes of the electrical signals due to continued hydration of the soil particles until a stable state is reached.

- After foam injection ceased, the resistivity increased due to the reduced number and thickness of the water films between gas bubbles during foam coalescence and drainage. The resistivity during bubble coalescence and breakage is still much lower than the baseline values of the original sediment due to enhanced moisture content of the sediments. The electrical resistivity response to foam injection and subsequent transformation was similar for both samples tested, suggesting its suitability for monitoring foam behavior in porous medium of different moisture retention capacities.
- A distinct phase and imaginary conductivity signature was observed for natural sediment grains during foam injection and transformation. These responses are indicative of the dynamics of the water films on sediment grains and between gas bubbles within the pore spaces. The different magnitude and behavior of the polarization behaviors between Ottawa sand and Hanford sediments highlighted the important role of sediment characteristics (texture, initial saturation, particle size distribution, etc) on polarization signals.
- TDR measurements were useful for estimating moisture content changes associated with foam injection and subsequent drainage. TDR data were useful for providing estimates of moisture content but were not sensitive to subtle changes in local redistribution of moisture and water films within the pore structures.

It is worthy to note that different geophysical attributes (resistivity, phase, dielectric constant) revealed different sensitivities to the various stages of foam injection. For example, while resistivity change during foam injection was significant and can be used to track foam injection process, concurrent phase change was small and could not be used for tracking foam injection. However, phase responses have demonstrated potential for tracking critical biogeochemical transformations in other studies and are expected to be

useful for monitoring long term geochemical transformations after foam injection has stopped. Our study suggests that the joint use of multiple monitoring methods, in this case complex resistivity and TDR, should greatly reduce interpretation uncertainty and improve process understanding associated with foam remediation.

Though our study, we have demonstrated the sensitivity of both electrical and TDR methods to foam injection and evolution in unsaturated porous media and the utility of these methods to monitor foam assisted remedy delivery for vadose zone remediation. However, foam-based remediation monitoring using geophysical methods is more complex than the study investigated here for two reasons: (1) the remediation treatments will lead to more complex (bio)geochemical reactions that can alter the pore and interfacial properties and concomitantly, the geophysical response. For example, we expect the time-lapse phase response to be potentially useful for studying longer term biogeochemical transformation occurring on sediment grains due to foam injection. (2) The ratio of the geophysical measurement support scale to the characteristic scale of the foam distribution or remediation process is much larger at the field scale relative to the laboratory scales investigated here. This increased ratio will decrease the ability of the geophysical method to resolve sharp gradients or localized phenomena. Nevertheless, with the growing interest in using foam as a strategy to deliver remedial treatment into contaminated vadose zone environments, our study suggests that geophysical methods hold significant potential for monitoring foam-based remediation technologies and suggests that further research is warranted.

Acknowledgements

This research was supported by the U.S. Department of Energy, Office of Environmental Management, EM-30 Technology Innovation and Development Office and Richland Operations Office. Help from Elsa Cordova and Danielle Jansik at PNNL on site sediments and foam generation method is highly appreciated. We thank the help from associate editor Andrew Ramsburg. We also thank Dale Rucker and two anonymous reviewers for constructive comments. LBNL is operated by University of California for U.S. Department of Energy under contract DE-AC02-05CH11231.

Literature Cited

Archie, G.E. 1942. The electrical resistivity log as an aid in determining some reservoir characteristics: Transactions of the american institute of mineral. Metallurgy and Petroleum Engineers 146:54-62.

Binley, A., G. Cassiani, et al. 2002. Vadose zone flow model parameterisation using cross-borehole radar and resistivity imaging. Journal of Hydrology 267:147-159.

Birchak, J.R., C.G. Gardner, et al. 1974. High dielectric constant microwave probes for sensing soil moisture. Proceedings of the IEEE 62:93-98.

Birkerman, J.J. 1973. Foams. Springer-Verlag, Berlin.

Creux, P., J. Lachaise, et al. 2007. Specific cation effects at the hydroxide-charged air/water interface. Journal of physical chemistry C 111:3753-3755.

Daniels, J.J., B. Allred, et al. 2005. Hydrogeophysical case studies in the vadose zone, chapter 14. p. 413-440. *In* Y. Rubin, and S. Hubbard (ed.) Hydrogeophysics. Springer, The Netherland.

Glass, R.J., T.S. Steenhuis, et al. 1988. Wetting front instability as a rapid and far-reaching hydrologic process in the vadose zone. J. Contam. Hydrol. 3:207-226.

Hanson, A.T., B. Dwyer, et al. 1993. Remediation of chromium-containing soils by heap leaching: Column study. J. Environ. Eng. 119:825-841.

Hendrickx, J.M.H., and M. Flury. 2001. Uniform and preferential flow mechanisms in the vadose zone, chapter 5. *In* NRC (ed.) Conceptual Models of Flow and Transport in the Fractured Vadose Zone.

Hirasaki, G.J. 1989. The steam-foam process. Journal of Petroleum Technology 41:449-456.

Hubbard, S., Y. Rubin, et al. 1997a. Ground-penetrating-radar-assisted saturation and permeability estimation in bimodal systems. Water Resour. Res. 33:971-990.

Hubbard, Susan, Peterson, J.E., Majer, E.L., Zawislanski, P.T., Roberts, J., Williams, K.H. and Wobber, F., 1997b, Estimation of permeable pathways and water content using tomographic radar data, *The Leading Edge of Exploration*, 16(11), 1623-1628.

Hubbard, S.S., K.H. Williams, et al. 2008. Geophysical monitoring of hydrological and biogeochemical transformations associated with cr(vi) bioremediation. Environ. Sci. Technol. 42:3757-3765.

Knight, R. 1991. Hysteresis in the electrical resistivity of partially saturated sandstones. Geophysics 56:2139-2147.

Kowalsky, M.B., S. Finsterle, et al. 2005. Estimation of field-scale soil hydraulic and dielectric parameters through joint inversion of gpr and hydrological data. Water Resour. Res. 41:W11425, DOI: 10.1029/2005WRR004237.

Lambot, S., E.C. Slob, et al. 2006. Closed loop gpr data inversion for soil hydraulic and electric property determination. Geophys. Res. Lett. 33:L21405, doi:10.1029/2006GL027906.

Lesmes, D.P., and F.D. Morgan. 2001. Dielectric spectroscopy of sedimentary rocks. J. Geophys. Res. 106:13329-13346.

Looney, B.B., and R.W. Falta. 2000. Vadose zone science and technology solutions. Battelle Press, Columbus, OH.

Lyklema, J. 1995. Fundamentals of interface and colloid science. p. 3.208. Vol.2.

Manciu, M., and E. Ruckenstein. 2006. Ions at the air/water interface. J. Colloid Interface Sci. 304:541-544.

Parkhomenko, E.I. 1971. Electrification phenomena in rocks. Plenum Press, New Yrok.

Qafoku, N.P., C.C. Ainsworth, et al. 2007. Cr(vi) fate in mineralogically altered sediments by hyperalkaline waste fluids. Soil Science 172:598-613.

Qafoku, N.P., C.C. Ainsworth, et al. 2003. Effect of coupled dissolution and redox reactions on $cr(vi)_{aq}$ attenuation during transport in the hanford sediments under hyperalkaline conditions. Environ. Sci. Technol. 37:3640-3646.

Rubin, Y., and S. Hubbard. 2005. Hydrogeophysics. Springer,Water and Science Technology Library, The Netherlands.

Rucker, D.F., J.B. Fink, et al. 2011. Environmental monitoring of leaks using time lapsed long electrode electrical resistivity. Journal of Applied Geophysics 74:242-254.

Schwarz, G. 1962. A theory of the low-frequency dielectric dispersion of colloidal particles in electrolyte solution. J. Phys. Chem. 66.

Slater, L., and D.P. Lesmes. 2002. Electrical-hydraulic relationships observed for unconsolidated sediments. Water Resour. Res. 38:-.

Slater, L.D., J. Choi, et al. 2005. Electrical properties of iron-sand columns: Implications for induced polarization investigation and performance monitoring of iron-wall barriers. Geophysics 70:G87-G94.

Smith, D.H. 1988. Surfactant-based mobility control: Progress in miscible-flood enhanced oil recovery. [Online] Am. Chem. Soc., Washington, D.C.

Titov, K., A. Kemna, et al. 2004. Induced polarization of unsaturated sands determined through time domain measurements Vadose Zone J. 3:1160-1168.

Topp, G.C., J.L. Davis, et al. 1980. Electromagnetic determination of soil water content: Measurement in coaxial transmission lines. Water Resour. Res. 16:574-582.

Ulrich, C., and L. Slater. 2004. Induced polarization measurements on unsaturated, unconsolidated sands. Geophysics 69:762-771.

Vanhala, H. 1995. Laboratory technique for measurement of spectral induced polarization response of soil samples. Geophysical Prospecting 43:655-676.

Williams, K.H., A. Kemna, et al. 2009. Geophysical monitoring of coupled microbial and geochemical processes during stimulated subsurface bioremediation. Environ. Sci. Technol. DOI 10.1021/es900855j.

Williams, K.H., D. Ntarlagiannis, et al. 2005. Geophysical imaging of stimulated microbial biomineralization. Environ. Sci. Technol. 39:7592-7600.

Wong, J. 1979. An electrochemical model of the induced-polarization phenomenon in disseminated sulfide ores. Geophysics 44:1245-1265.

Wu, Y., J.B. Ajo-Franklin, et al. 2011. Geophysical monitoring and reactive transport modeling of ureolytically-driven calcium carbonate precipitation Geochem. Trans. 12.

Wu, Y., S.S. Hubbard, et al. 2010. On the complex conductivity signatures of calcite precipitation. J. Geophys. Res. 115:G00G04, doi:10.1029/2009JG001129.

Yan, W., C.A. Miller, et al. 2006. Foam sweep in fractures for enhanced oil recovery. Colloids Surf., A 282:348-359.

Zhong, L., M. Ankeny, et al. 2009. Research plan:Foam delivery of amendments to the deep vadose zone for metals and radionuclides remediation. Pacific Northwest National Laboratory, Richland, WA.

Zhong, L., N.P. Qafoku, et al. 2009. Foam delivery of calcium polysulfide to the vadose zone for chromium (vi) immobilization: A laboratory evaluation. Vadose Zone J. 8:976-985.

Zhong, L., J.E. Szecsody, et al. 2010. Foam delivery of amendments for vadose zone remediation: Propagation performance in unsaturated sediments. Vadose Zone J. 9:757-767.